C. Normalization Constants

In order to expand the fields of sources in the presence of the slotted screen, the eigenmodes must be normalized. This can be accomplished in a number of ways [3]. Only the final results are stated.

Let the transverse electric field of a TM_z mode corresponding to the mth radial solution and spectral number k_t be denoted by

$$\mathbf{E}_{\mathrm{TM}}^{e,o}(m,h) = \nabla_t \Phi_m^{e,o}(h, \cosh\mu, \cos\theta)$$

and the electric field of a TE_z mode corresponding to the mth radial solution and spectral number k_t by

$$\mathbf{E}_{\mathrm{TE}}^{e,o}(m,h) = \hat{\mathbf{z}} \times \nabla_t \Psi_m^{e,o}(h, \cosh\mu, \cos\theta).$$

Upon defining the inner product over the transverse cross-section S as follows

$$\langle \mathbf{A}, \mathbf{B} \rangle = \iint_S \mathbf{A} \cdot \mathbf{B} \quad ds$$

it can be shown that the following equations are true

$$\begin{aligned}
&\langle \mathbf{E}_{\mathrm{TM}}^{e}(m,h_1), \mathbf{E}_{\mathrm{TM}}^{e}(n,h_2) \rangle \\
&\quad = \frac{\pi}{2} k_{t1} M_m^o(h_1)[Jo_m'(h_1,1)^2 + No_m'(h_1,1)^2] \\
&\quad \times \delta(k_{t1} - k_{t2})\delta_{mn} \\
&\langle \mathbf{E}_{\mathrm{TM}}^{o}(m,h_1), \mathbf{E}_{\mathrm{TM}}^{o}(n,h_2) \rangle \\
&\quad = \frac{\pi}{2} k_{t1} M_m^o(h_1)[Jo_m'(h_1,1)]^{-2} \delta(k_{t1} - k_{t2})\delta_{mn} \\
&\langle \mathbf{E}_{\mathrm{TE}}^{e}(m,h_1), \mathbf{E}_{\mathrm{TE}}^{e}(n,h_2) \rangle \\
&\quad = \frac{\pi}{2} k_{t1} M_m^e(h_1)[Je_m(h_1,1)^2 + Ne_m(h_1,1)^2] \\
&\quad \times \delta(k_{t1} - k_{t2})\delta_{mn} \\
&\langle \mathbf{E}_{\mathrm{TE}}^{o}(m,h_1), \mathbf{E}_{\mathrm{TE}}^{o}(n,h_2) \rangle \\
&\quad = \frac{\pi}{2} k_{t1} M_m^e(h_1)[Je_m(h_1,1)]^{-2} \delta(k_{t1} - k_{t2})\delta_{mn}
\end{aligned}$$

where $\delta(\cdot)$ is the delta function, δ_{mn} is the Kronecker symbol, and normalization constants $M_m^{e,o}$ are defined in [4].

D. Characteristic Modes for the Slot

The characteristic slot-field modes defined in [2] can be shown to correspond to the tangential field distributions of the eigenmode solutions stated above, evaluated at $\mu = 0$. For example, the characteristic TE_z aperture modes for a given value of k_t are obtained as

$$\mathbf{E}_{\mathrm{TE}}^{e}(m,h,1,x) = \hat{\mathbf{x}} \frac{Se_m(h, 2x/a)}{\sqrt{(\frac{a}{2})^2 - x^2}}; \quad -\frac{a}{2} \le x \le \frac{a}{2}$$

where the substitution $\frac{1}{2}a\cos\theta = x$ was made. Numerical evaluation of $Se_m(h, 2x/a)$ can be carried out using a number of software packages, e.g., [7].

The characteristic values, denoted by $b_m(k_t)$ in [2] ($\lambda_m(k_t)$ in [1]) can be explicitly written as follows

$$b_m(k_t) = \frac{Ne_m(h,1)}{Je_m(h,1)}.$$

The approximate $b_m(k_t)$ values derived in [2] represent the first terms in the series expansion of the preceding equation for small values of h.

REFERENCES

[1] M. Mongiardo and T. Rozzi, "Continuous spectrum, characteristic modes, and leaky waves of open waveguides," *IEEE Trans. Microwave Theory Tech.*, vol. 41, no. 8, Jan. 1993.
[2] K. Y. Kabalan, R. F. Harrington, H. A. Auda, and J. R. Mautz, "Characteristic modes for slots in a conducting plane, TE case," *IEEE Trans. Antennas Propagat.*, vol. AP-35, no. 2, Jan. 1987.
[3] L. B. Felsen and N. Marcuvitz, *Radiation and Scattering of Waves*. Engelwood Cliffs, NJ: Prentice-Hall, 1973.
[4] P. M. Morse and H. Feshbach, *Methods of Theoretical Physics*. New York: McGraw-Hill, 1953.
[5] J. Meixner and F. W. Schäfke, *Mathieusche Funktionen und Sphäroidfunktionen*. Berlin: Springer-Verlag, 1954.
[6] A.-M. A. El-Sherbiny, "Cutoff wavelength of ridged, circular, and elliptic guides," *IEEE Trans. Microwave Theory Tech.*, vol. MTT-21, no. 1, Jan. 1973.
[7] IMSL Mathematics Fortran Library, User's Manual, version 10.0.

Electrostatic Potential Through a Circular Aperture in a Thick Conducting Plane

Jung H. Lee and Hyo J. Eom

***Abstract*—The electrostatic potential through a circular aperture in a thick conducting plane is examined. The Hankel transform is applied to express the scattered potential in the spectral domain and the boundary conditions are enforced to obtain simultaneous equations for the transmitted potential inside the thick conducting plane. The simultaneous equations are solved to represent the transmitted and scattered potentials in series forms. Numerical computations are performed to illustrate the behavior of polarizability in terms of the aperture size. The numerical comparisons to other available data show excellent agreement. The presented series solution is fast convergent so that it is very efficient for numerical computation.**

I. INTRODUCTION

Electrostatic potential through a circular aperture in a thin conducting plane has been of considerable interest in the area of microwaves [1]–[3]. The potential penetration through a circular aperture in a thick conducting plane has been studied with the variational technique [4]. Although the solution in [4] fairly well agrees with the measurement data, it is also of interest to obtain another rigorous exact solution. The motivation of the present study is to develop such a solution by using the Hankel transform and the mode-matching used in [5]. The solution presented in this paper is in simple convergent series so that it is not only exact but also computationally very efficient. The organization of the paper is as follows: In the next section, we represent the scattered potential in the spectral domain and perform the numerical calculations. A brief summary is given in Conclusion.

II. POTENTIAL REPRESENTATIONS AND BOUNDARY CONDITIONS

In region (I) ($z > 0$), an incident potential Φ^i impinges on a circular aperture (radius: a, depth: d) in a thick conducting plane at zero potential (see Fig. 1). Regions (II) ($-d < z < 0, r < a$) and (III) ($z < -d$) denote the circular aperture and the lossless half-space, respectively. In region (I) the total potential consists of the

Manuscript received December 30, 1994; revised November 12, 1995.
The authors are with the Department of Electrical Engineering, Korea Advanced Institute of Science and Technology, 373-1, Kusong Dong, Yusung Gu, Taejon, Korea.
Publisher Item Identifier S 0018-9480(96)01459-7.

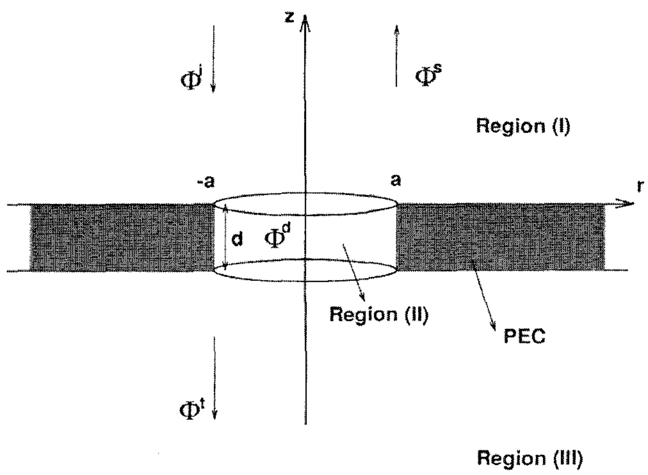

Fig. 1. Problem geometry.

incident and scattered potentials as

$$\Phi^i(r,z) = z \tag{2.1}$$

$$\Phi^s(r,z) = \int_0^\infty \tilde{\Phi}^s(\zeta) J_0(\zeta r) e^{-\zeta z} \zeta d\zeta \tag{2.2}$$

where $J_0(\cdots)$ is the zeroth order Bessel function and $\tilde{\Phi}^s(\zeta)$ is the Hankel transform of $\Phi^s(r,0)$ defined as $\tilde{\Phi}^s(\zeta) = \int_0^\infty \Phi^s(r,0) J_0(\zeta r) r dr$. The properties of the Hankel transform are summarized in [6]. In region (II) the total potential is given by the modal series with coefficients b_n and c_n where the discrete radial modes are determined by $J_0(k_n a) = 0$

$$\Phi^d(r,z) = \sum_{n=1}^{\infty} [b_n \sinh k_n(z+d) + c_n \cosh k_n(z+d)] J_0(k_n r). \tag{2.3}$$

In region (III) the total transmitted potential is

$$\Phi^t(r,z) = \int_0^\infty \tilde{\Phi}^t(\zeta) J_0(\zeta r) e^{\zeta(z+d)} \zeta d\zeta. \tag{2.4}$$

To determine unknown coefficients b_n and c_n, it is necessary to enforce the boundary conditions which require continuity of the potential and its normal derivative across the aperture

$$\Phi^i(r,0) + \Phi^s(r,0) = \Phi^d(r,0), \quad r < a \tag{2.5}$$

$$= 0, \quad r > a. \tag{2.6}$$

Applying the Hankel transform to (2.5) and (2.6)

$$\tilde{\Phi}^s(\zeta) = \sum_{n=1}^{\infty} (b_n \sinh k_n d + c_n \cosh k_n d) \times \left[\frac{-a k_n J_0(\zeta a) J_1(k_n a)}{\zeta^2 - k_n^2}\right]. \tag{2.7}$$

Second

$$\frac{\partial}{\partial z}[\Phi^i(r,z) + \Phi^s(r,z)]_{z=0} = \frac{\partial}{\partial z}[\Phi^d(r,z)]_{z=0}, \quad r < a. \tag{2.8}$$

Utilizing (2.1)–(2.3), (2.8) may be rewritten as

$$1 - \int_0^\infty \tilde{\Phi}^s(\zeta) J_0(\zeta r) \zeta^2 d\zeta = \sum_{n=1}^{\infty} [b_n \cosh k_n d + c_n \sinh k_n d] k_n J_0(k_n r), \quad r < a. \tag{2.9}$$

It is possible to form a linear system for b_n and c_n by applying an orthogonal property $\int_0^a J_0(k_n r) J_0(k_p r) r dr = \frac{a^2}{2}[J_1(k_p a)]^2 \delta_{np}$ to (2.9) where δ_{np} is the Kronecker delta. Substituting (2.7) into (2.9), multiplying (2.9) by $J_0(k_p r) r, (p = 1, 2, 3, \cdots)$ and integrating with respect to r from 0 to a

$$\frac{a J_1(k_p a)}{k_p} - \sum_{n=1}^{\infty} (b_n \sinh k_n d + c_n \cosh k_n d) \alpha_{np} I_{np} = \frac{a^2}{2} k_p [J_1(k_p a)]^2 (b_p \cosh k_n d + c_p \sinh k_n d) \tag{2.10}$$

where

$$\alpha_{np} = a^2 k_n k_p J_1(k_p a) J_1(k_n a) \tag{2.11}$$

$$I_{np} = \int_0^\infty \frac{J_0^2(\zeta a) \zeta^2}{(\zeta^2 - k_n^2)(\zeta^2 - k_p^2)} d\zeta. \tag{2.12}$$

Since the integrand of (2.12) is fast-decaying as ζ goes to infinity, the numerical evaluation of (2.12) is very efficient. Similarly from the boundary conditions at $z = -d$ we obtain

$$\sum_{n=1}^{\infty} c_n \alpha_{np} I_{np} = \frac{a^2}{2} b_p k_p [J_1(k_p a)]^2. \tag{2.13}$$

From (2.10) and (2.13), we obtain the matrix equation for c_n and b_n

$$\begin{bmatrix} \Psi_1 & \Psi_2 \\ \Psi_3 & \Psi_4 \end{bmatrix} \begin{bmatrix} B \\ C \end{bmatrix} = \begin{bmatrix} \Gamma \\ 0 \end{bmatrix} \tag{2.14}$$

where B and C are column vectors consisting of elements b_n and c_n, respectively, and $\Psi_1, \Psi_2, \Psi_3, \Psi_4$, and Γ elements are

$$\psi_{1,np} = \alpha_{np} \sinh(k_n d) I_{np} + \frac{a^2}{2} k_n \cosh(k_n d) [J_1(k_n a)]^2 \delta_{np} \tag{2.15}$$

$$\psi_{2,np} = \alpha_{np} \cosh(k_n d) I_{np} + \frac{a^2}{2} k_n \sinh(k_n d) [J_1(k_n a)]^2 \delta_{np} \tag{2.16}$$

$$\psi_{3,np} = \frac{a^2}{2} k_n [J_1(k_n a)]^2 \delta_{np} \tag{2.17}$$

$$\psi_{4,np} = -\alpha_{np} I_{np} \tag{2.18}$$

$$\gamma_p = \frac{a J_1(k_p a)}{k_p}. \tag{2.19}$$

Solving (2.14) for B and C, we have

$$B = (\Psi_1 \Psi_4 \Psi_3^{-1} - \Psi_2)^{-1} \Psi_3^{-1} \Psi_4 \Gamma$$
$$C = -(\Psi_1 \Psi_4 \Psi_3^{-1} - \Psi_2)^{-1} \Gamma. \tag{2.20}$$

Note that the electric polarizability defined in [3] is

$$\chi(z) \equiv 4\pi \int_0^a \Phi^d(r,z) r dr \tag{2.21}$$

$$= 4\pi a \sum_{n=1}^{\infty} [b_n \sinh k_n(z+d) + c_n \cosh k_n(z+d)] J_1(k_n a)/k_n. \tag{2.22}$$

Three limiting cases are:

1) When $d = 0$ (thin circular aperture), $B = \frac{1}{2}\Psi_1^{-1}\Gamma$ and $C = \frac{1}{2}\Psi_2^{-1}\Gamma$;
2) When region (III) consists of a perfect-conducting plane at zero potential (circular pit), $B = \Psi_1^{-1}\Gamma, C = 0$;
3) When $d = \infty$ (infinite circular pipe), $B = \frac{1}{2}\Psi_1^{-1}\Gamma, C = B$.

TABLE I
CONVERGENCE RATE OF $|b_n|$ AND $|c_n|$ VERSUS n FOR THE THICK CIRCULAR APERTURE WITH $a = 2$

d/a	0.1		0 5		1	
n	$\|b_n\|$	$\|c_n\|$	$\|b_n\|$	$\|c_n\|$	$\|b_n\|$	$\|c_n\|$
1	0.525710	0.632149	0 202444	0 237521	0 060972	0 071151
2	0.103520	0.170552	0.004229	0 025546	0.002128	0.004010
3	0 031176	0.079210	0 005764	0.009175	0.002008	0 002163
4	0.008332	0.045435	0.005445	0.005917	0 001622	0.001624
5	0.000582	0.029456	0 004510	0.004582	0.001296	0 001296
6	0 004330	0.020786	0 003761	0 003773	0 001072	0.001072

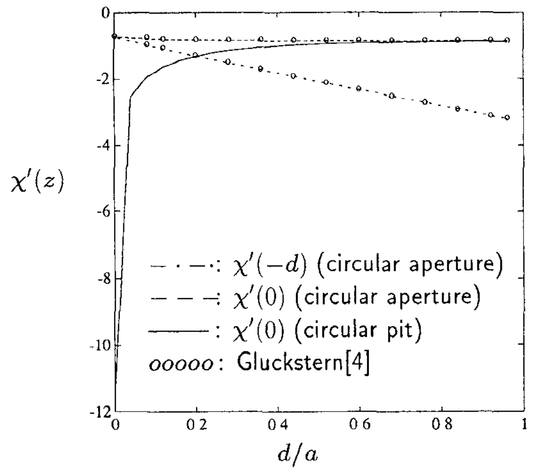

Fig. 2. Normalized polarizability as a function of aperture thickness.

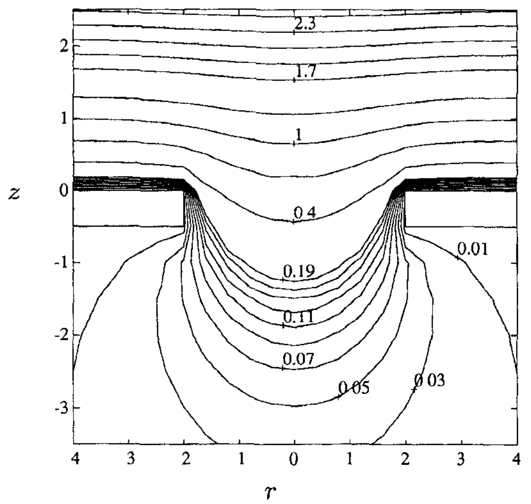

Fig. 3. Equipotential contour when $d/a = 0.25$.

In order to show the convergence rate of our series solution, we tabulate $|b_n|$ and $|c_n|$ in Table I for the thick circular aperture, demonstrating that our series solution converges rapidly. To check the accuracy of our formulation, we plot the normalized polarizability $\chi'(z) = \ln[3\chi(z)/(8a^3)]$ for the circular aperture at $z = 0, -d$ in Fig. 2, thus confirming excellent agreements between out results and [4]. Note that the normalized polarizability is independent of a. We use $n = 6$ in (2.20) to achieve the numerical convergence. The typical CPU time for solving (2.20) is about 45 msec on a Sun-workstation model SPARC-20. Our computation shows that $\chi'(0)$ for the circular pipe is approximately -0.86. Note that $\chi'(0)$ for the circular pit approaches that for the circular aperture within 1% error when $d/a > 0.5$. This is because the bottom metallic surface at $z = -d$ has a diminishing effect of the polarizability since it is receding from the aperture. This is also evident in the fact that the polarizability at $z = -d$ for the circular aperture becomes increasingly small as d increases. Also note that $\chi'(0)$ for the circular pit approaches 0 when $d/a \to 0$ since it is a limiting case of a nonexistent aperture. For the sake of illustration, we show the equipotential contour for the thick aperture in Fig. 3 which depicts how the incident potential penetrates into a thick circular aperture with $d/a = 0.25$.

III. CONCLUSION

The electrostatic potential distribution through a thick circular aperture is investigated. A simple series solution is obtained using the Hankel transform and the polarizability for the aperture is numerically evaluated. The presented solution converges rapidly so that it is very efficient for numerical computation.

REFERENCES

[1] E. E. Okon and R. F Harrington, "The polarizabilities of electrically small apertures of arbitrary shape," *IEEE Trans. Electromag. Compat.*, vol. EMC-23, no. 4, pp. 359–366, Nov. 1981.

[2] K. F Casey, "Low-frequency electromagnetic penetration of loaded apertures," *IEEE Trans. Electromag. Compat.*, vol. EMC-23, no. 4, pp. 367–377, Nov. 1981

[3] R. L. Gluckstern, R. Li, and R. K. Cooper, "Electric polarizability and magnetic susceptibility of small holes in a thin screen," *IEEE Trans. Microwave Theory Tech.*, vol. 38, no. 2, pp. 186–191, Feb. 1990.

[4] R. L. Gluckstern and J. A. Diamond, "Penetration of fields through a circular hole in a wall of finite thickness," *IEEE Trans. Microwave Theory Tech.*, vol. 39, no. 2, pp. 274–279, Feb. 1991.

[5] H. J. Eom and T. J. Park, "A series solution for acoustic radiation from a flanged circular pipe," *Acustica*, vol. 80, no. 1, pp. 315–316, 1994.

[6] I. N. Sneddon, *The Use of Integral Transform.* New York: McGraw-Hill, 1972, pp. 298–317.